

The effect of the melt thermal gradient on the size of the constitutionally supercooled zone

This content has been downloaded from IOPscience. Please scroll down to see the full text.

2016 IOP Conf. Ser.: Mater. Sci. Eng. 117 012001

(<http://iopscience.iop.org/1757-899X/117/1/012001>)

View [the table of contents for this issue](#), or go to the [journal homepage](#) for more

Download details:

IP Address: 105.235.144.70

This content was downloaded on 03/04/2016 at 14:40

Please note that [terms and conditions apply](#).

The effect of the melt thermal gradient on the size of the constitutionally supercooled zone

A Prasad^{1,a}, L Yuan^{2,b}, P D Lee^{2,c}, M Easton^{3,d} and D StJohn^{1,e}

¹ Centre for Advanced Materials Processing and Manufacturing, The University of Queensland, Brisbane, Australia

² The Manchester X-ray Imaging Facility, School of Materials, The University of Manchester, Oxford Rd., Manchester, M13 9PL, UK

³ School of Aerospace, Mechanical and Manufacturing Engineering, RMIT University, Melbourne, Australia

Email: ^aa.prasad3@uq.edu.au, ^blang.yuan@manchester.ac.uk, ^cpeter.lee@manchester.ac.uk, ^dmark.easton@rmit.edu.au, ^ed.stjohn@uq.edu.au

Abstract. Recent verification of the analytical Interdependence model by a numerical solidification model (μ MatIC) confirmed the critical role of constitutional supercooling (CS) in achieving sufficient undercooling to trigger successful nucleation events. The location of the maximum amount of CS (ΔT_{CSmax}) is some distance from the interface of the previously growing grain and this distance contributes to the final as-cast grain size. The effect of the thermal gradient, G , on the size of the CS zone (CSZ) was neglected in that work. However, G is expected to affect the size of the CSZ (i.e. the length of the CSZ, x'_{CSZ} , and the location of ΔT_{CSmax} , x'_{CSmax}). This investigation assesses the effect of G on x'_{CSZ} and x'_{CSmax} . A range of G values is introduced into both the analytical and the numerical models to obtain a correlation between the value of G and the dimensions of the CSZ. The result of a test case from the analytical model shows that x'_{CSmax} initially decreases rapidly and then decreases gradually approaching zero at very high values of G . Independent of the analytical model, the results from the numerical model replicate the trend obtained from the analytical model.

1. Introduction

The Interdependence model, which can predict the grain size of a casting, states that a new grain is nucleated when the amount of constitutional supercooling (ΔT_{CS}) of an already growing grain is large enough to activate an inoculant particle, which requires a certain minimum undercooling [1-4]. Equation 1 shows the key distances of the Interdependence model for a near-zero thermal gradient at large distances from the advancing solid-liquid (S-L) interface (for example T_{A1} in figure 1).

$$d_{gs} = x_{cs} + x'_{dl} + x_{sd} \quad (1)$$

Here d_{gs} is the predicted grain size, x_{cs} is the growth radius of the already growing grain, x'_{dl} the solute diffusion length ahead of the growing grain and x_{sd} the separation distance of the inoculant particles. In the original model [4] the expression for x_{cs} contains a 'z' term which sets the additional CS required for subsequent nucleation events where z is a function of the thermal gradient present in the system. However, no detailed analysis of the thermal gradient has been undertaken and z assumes a pre-set user-defined value. The most appropriate value of z can only be determined following a detailed analysis of the effect of thermal gradient on the CS zone (CSZ). Here the size of the CSZ is



described as the length x'_{CSZ} ahead of the S-L interface where ΔT_{CS} is positive, as well as the position, x'_{CSmax} , of ΔT_{CSmax} within this length. Note that x'_{CSZ} is not equal to x'_{dl} , the diffusion length as defined previously [4], in figure 1. x'_{dl} is independent of G and thus x'_{CSZ} can be smaller or larger than x'_{dl} depending on the value of G . The prime symbol is used because x' is the distance from the S-L interface whereas x (for example x_{CS} in figure 1) is measured from the point of nucleation [4].

As a first step the Interdependence model is used to qualitatively study the effect of G on the size of CSZ. The qualitative analysis from the analytical model is compared with the results from the μ MatIC numerical model [5, 6]. Some preliminary results from this analysis are presented in this paper.

Figure 1 shows the equilibrium temperature, T_E , and the actual melt temperature, T_A , ahead of a growing grain. ΔT_{CS} is given by $(T_E - T_A)$ and T_E changes along the length ahead of the growing grain governed by the solute diffusion from the growing S-L interface. In the case of zero thermal gradient, given by line T_{A1} in figure 1, ΔT_{CS} is simply $T_E - T_{A1}$. Note that when $T_A = 0$ (i.e. T_{A1}) x'_{CSZ} is infinite. The point of maximum supercooling, ΔT_{CSmax} , is given by the distance from the S-L interface to where T_E first attains its largest value. However, a thermal gradient is usually present in castings from the periphery to the thermal centre. The effect of the thermal gradient is usually studied in directional solidification experiments and numerical models. Within these, there are limited studies on the effect of thermal gradient on the nucleation of new grains. Dong-Lee [7] and Badillo-Beckermann [8] briefly mentioned the role of G in nucleation ahead of columnar grains in their study of the columnar to equiaxed transition (CET) and highlighted the importance of the influence of G on CS.

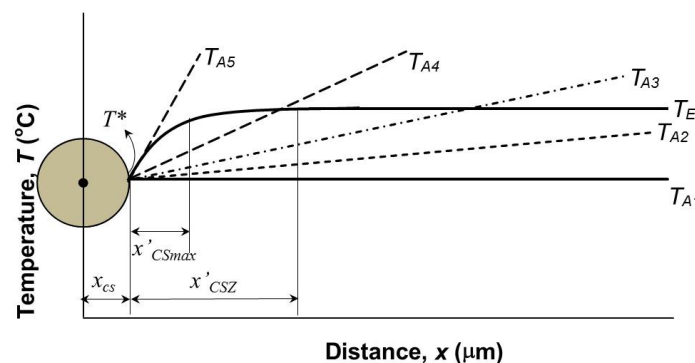


Figure 1. Schematic representation of the CSZ as described by the Interdependence model with varying degrees of thermal gradient, G . The approximate lengths of x'_{CSZ} (where ΔT_{CS} is positive), and x'_{CSmax} (corresponding to ΔT_{CSmax}) for T_{A4} are shown in the figure.

Assuming that the inoculant particle separation distance, x_{sd} , does not change in equation 1, the variation of the nucleation distance of new grains becomes a function of the sum of the first two terms only. Figure 1 shows this scenario conceptually for non-zero thermal gradients. The schematic representation shows that increasing G would decrease x'_{CSZ} approaching 0 at high G values. x'_{CSZ} is the total distance from the interface where ΔT_{CS} is still positive. The changing shape of $T_E(x)$ near the interface suggests that between the S-L interface and x'_{CSZ} there exists a distance, x'_{CSmax} , where ΔT_{CS} is at its maximum value ΔT_{CSmax} . Both x'_{CSZ} and x'_{CSmax} are shown schematically for T_{A4} in figure 1. To verify this, the effect of thermal gradient is studied in two ways. An analytical expression is developed which relates x'_{CSZ} and x'_{CSmax} to the thermal gradient, G . A numerical model, μ MatIC [5, 6], is also used to simulate the solidification of a grain in the presence of a thermal gradient and x'_{CSZ} is estimated. Finally, the results from the analytical and μ MatIC models are compared.

2. Analytical solution

Equation 2 shows the general form describing the equilibrium temperature, $T_E(x)$. This was derived by combining the expressions for T_E and $C_l(x)$ [4]. In the case of zero thermal gradient ΔT_{CSmax} is equal to T_{liq} (the liquidus temperature of the alloy) minus T^* (the temperature at the S-L interface) at some distance from the interface where the solute concentration attains the alloy composition C_0 . In the case of non-zero thermal gradient, the length of positive ΔT_{CS} , i.e. x'_{CSZ} , is equal to $T_E - T_A$, if T_A is known. However, similar to T_E , T_A changes with distance, the general expression for which is given in equation 3. In these two equations, C_0 is the alloy composition, m is the slope of the liquidus line of the alloy system in question, $C_l^*(x')$ is the solute concentration at the interface and G represents the general thermal gradient term. By determining $T_E(x') - T_A(x')$, it can be shown that ΔT_{CS} is a function of distance, $\Delta T_{CS}(x')$, as shown in Equation 4:

$$T_E(x') = T_{liq} + m \left\{ (C_l^*(x') - C_0) e^{-\frac{V}{D}x'} \right\} \quad (2)$$

$$T_A(x') = T^* + Gx' \quad (3)$$

$$\Delta T_{CS}(x') = T_E(x') - T_A(x') = T_{liq} + m \left\{ (C_l^*(x') - C_0) e^{-\frac{V}{D}x'} \right\} - T^* - Gx' \quad (4)$$

By changing the $[m(C_l^*(x') - C_0)]$ term in equation 4 to $(T^* - T_{liq})$, the following is obtained:

$$\Delta T_{CS}(x') = T_E(x') - T_A(x') = \left\{ (T^* - T_{liq}) \left(e^{-\frac{V}{D}x'} - 1 \right) \right\} - Gx' \quad (5)$$

Equation 5 states that for any value of G , ΔT_{CS} is zero when x' is 0 (i.e. at the S-L interface) and for $G = 0$, ΔT_{CS} is $(T_{liq} - T^*)$ from x'_{dl} to ∞ . For $G > 0$, $\Delta T_{CS} = 0$ at some x' for a given value of G . x'_{CSZ} can now be evaluated for values of G (>0) and is given by the distance between the points where $\Delta T_{CS} = 0$. Furthermore, ΔT_{CSmax} corresponding to x'_{CSmax} lies between the two extremes where $\Delta T_{CS} = 0$. x'_{CSmax} can be evaluated by mathematically maximizing the expression for $\Delta T_{CS}(x')$ in equation 5 with respect to the distance x' . This is shown in equation 6. Note that T^* has been assumed to be constant.

$$x'_{CSmax} = -\frac{D}{V} \ln \left\{ \left(\frac{GD}{V} \right) \cdot \frac{1}{T_{liq} - T^*} \right\} \quad (6)$$

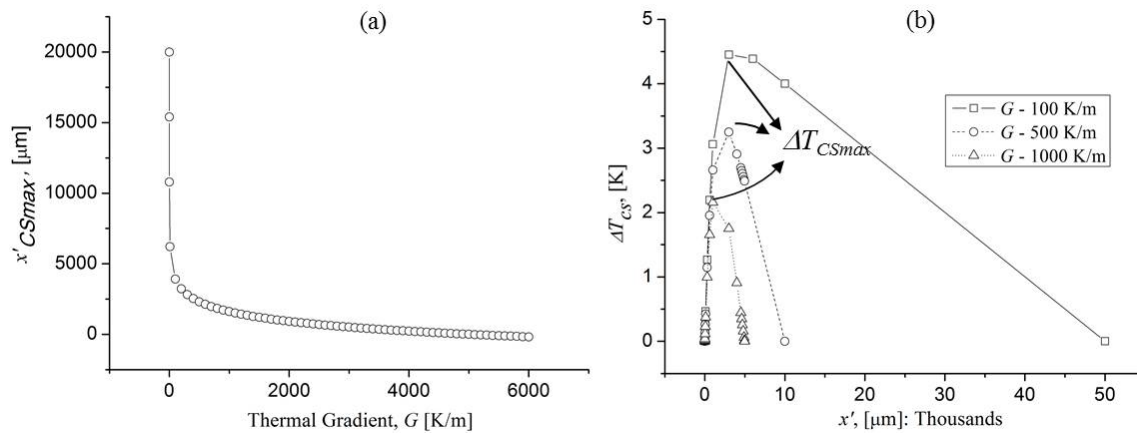


Figure 2. (a) x'_{CSmax} , the location of ΔT_{CSmax} , shown as a function of thermal gradient. At high G values, x'_{CSmax} approaches zero. (b) ΔT_{CS} ($= T_E(x') - T_A(x')$) as a function of distance, x' , for different G . As G increases x'_{CSZ} , the total distance of positive ΔT_{CS} , and ΔT_{CSmax} decrease.

Equation 5 was used to plot the change in ΔT_{CS} with distance for a given thermal gradient G , and equation 6 was used to assess the effect of thermal gradient on the distance at which ΔT_{CSmax} is attained. Table 1 shows the values used. Figure 2a shows x'_{CSmax} corresponding to ΔT_{CSmax} as a function of the thermal gradient, G . As the thermal gradient increases, x'_{CSmax} decreases exponentially due to the logarithmic term in equation 6: faster at low G values then decreasing gradually at higher G . At high G values, x'_{CSmax} tends to 0. Figure 2b shows the variation in ΔT_{CS} with distance x' from the S-L interface and confirms the observations made in the previous paragraph. The peak value of ΔT_{CS} within x'_{CSZ} is ΔT_{CSmax} . As G increases x'_{CSZ} decreases and so does ΔT_{CSmax} .

3. Numerical solution: The μ MatIC model

The numerical model was used to simulate a centrally placed single grain growing in a 5mm x 5mm computational domain with a left to right thermal gradient G (i.e. the temperature increases from left to right). Details of the model and its simulations are provided elsewhere [5-7, 9-11]. The alloy system modelled was Al-7%Si with an initial temperature of 887 K (614°C) at the left hand side. Five simulations were performed over a range of G , as given in table 1. The simulation time for each run was 86 s with a cooling rate of 0.3 K/s (calculated in the model as $G.V$ where V is the pulling velocity in a directional solidification experiment). The time chosen was to ensure that the right hand side of the computational domain reached a temperature lower than the alloy liquidus, T_{liq} . Following the simulation the grain size and the solute diffusion length ahead of the growing grain was estimated at 25, 50, 75 and 86 s.

Table 1. Values used in equations 5 and 6. Note that the analytical model was used as a test case only for the purposes of this paper. The G values used in the numerical model are also shown.

Item	Description	Value	Units
T_{liq}	Liquidus of the alloy system	913	[K]
T^*	S-L interface temperature	908	[K]
G (analytical)	Thermal gradient	$\sim 0 - 10000$	[K/m]
D (analytical)	Solute diffusion in the liquid	$2e-9$	[m ² /s]
v (analytical)	Interface growth rate	$2e-6$	[m/s]
G (numerical)	Thermal gradient in μ MatIC	0, 100, 1000, 2000, 5000	[K/m]

* Note that the absolute values of T_{liq} and T^* are not important in equation 5.

Figure 3 shows the solutal profile ahead of the growing grain which shows an exponential decay with distance. Close to the interface, between $G = 100$ to 2000 K/m, the solute concentration is high, which decreases with increasing G values, i.e. $C_{G=1000} < C_{G=100}$. At large distances, profiles from all G values attain the alloy composition of 7%. The solute concentration at any point was translated to an equilibrium liquidus temperature, T_E , at that location. Similar to equation 4, the ΔT_{CS} related to the actual temperature can be obtained by subtracting the location dependent thermal gradient $T_A(x)$ from the CS governed equilibrium liquidus temperature at a given location. This is shown in figure 3b for $G = 5000$ K/m at $t = 50$ s. T_E , T_A and ΔT_{CS} are shown in the plot. The solute concentration is denoted as $C_E - C_0$. These operations were carried out for all the numerical simulation results.

At $G = 5000$ K/m the concentration ahead of the interface is low. Figure 4b shows the time varying grain growth for $G = 5000$ K/m. It shows that at $t = 50$ s grain growth is in its very initial stages and, hence, the interfacial solute concentration is much lower than that for other G values. On the other hand, at $G = 0$, the concentration is very high adjacent to the S-L interface which then exponentially decreases. Figure 4c shows the growth of a grain at $t = 50$ s with increasing G from left to right. At $G = 0$ the growth is much more advanced than at higher thermal gradients. The reduced growth with increasing thermal gradient can be explained by the higher temperatures close to the interface when G is high. These higher temperatures ahead of the S-L interface also significantly reduce the growth of the dendrite along the $+x'$ direction.

The ΔT_{CS} profile ahead of the growing grain in figure 3b follows that of the analytical model with a convex-up shape. See figure 1 for a schematic representation and figure 2 for analytical results.

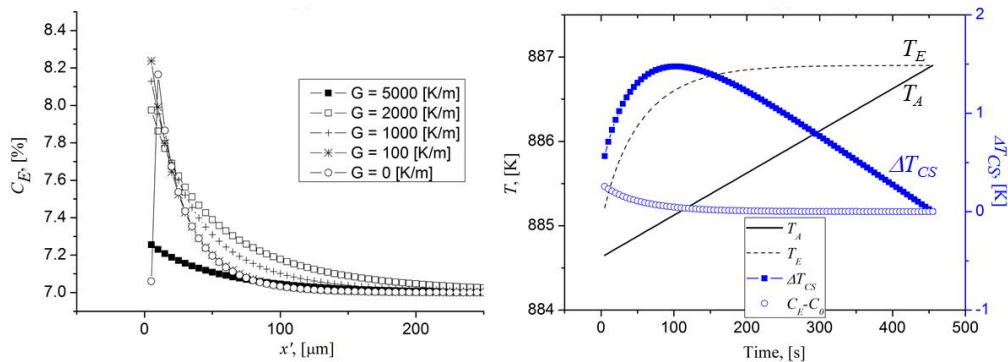


Figure 3. (a) Plot of the solute profile ahead of a growing grain for different G values at $t = 50$ s. (b) The corresponding ΔT_{CS} over distance x' , evaluated as $T_E - T_A$.

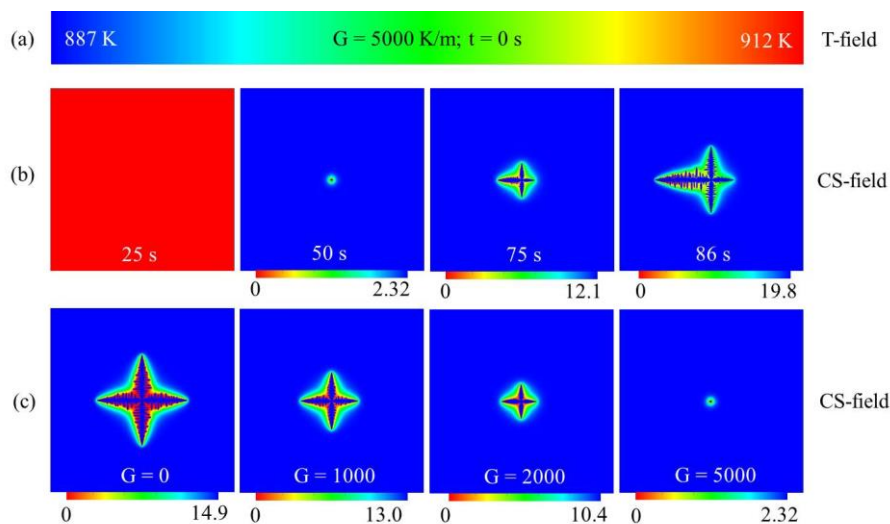


Figure 4. (a) The temperature field at $t = 0$ s for $G = 5000$ K/m. (b) Grain growth with increasing time for $G = 5000$ K/m shown in a CS field. (c) The dendrite size at $t = 50$ s (also in CS-field) for increasing values of G from left to right. As G increases the time required for a given amount of grain growth increases. In both figures (b) and (c), the higher temperatures on the right hand side reduce the amount of growth in the x' direction. The scale bar shows the ΔT_{CS} values ahead of the growing grains. As t increases or G decreases ΔT_{CSmax} increases.

4. Discussion and conclusions

x'_{CSmax} calculated from the numerical simulations as explained above is plotted for different G values in figure 5a. This is done for two times, $t = 40$ s and 50 s. As G increases, x'_{CSmax} decreases. At $G = 5000$ K/m, the result for $t = 40$ s does not show any value as no solidification had commenced by that time. At 2000 K/m the x'_{CSmax} values for the two times are almost the same. At lower G values (1000 K/m or lower), there is already significant growth by $t = 40$ s (cf figure 4 which shows lower G values produce larger dendrites).

Comparison between the analytical and numerical results is presented in Figure 5b. It shows that the general trend of the analytical and the numerical models are similar with good agreement between the two at high G values. With increasing G the x'_{CSmax} corresponding to ΔT_{CSmax} decreases

exponentially. Moreover, the numerical model shows a decrease in ΔT_{CS} with increasing G . Thus, the conceptual representation in figure 1 is confirmed by both approaches. The analytical solution may overestimate x'_{CSmax} particularly at low G values, possibly due to the assumption of a constant interfacial temperature T^* . This effect is confirmed by plotting the data for a lower difference between $T_{liq} - T^*$ (i.e. 2K in equation 5) in figure 5b, which shows a better agreement with the numerical solution compared to $T_{liq} - T^* = 5$ K. Moreover, with grain growth, the S-L interface moves and its position changes with respect to x' . Thus, further development needs to calculate changes in T^* rather than assuming it to be a constant as is done here.

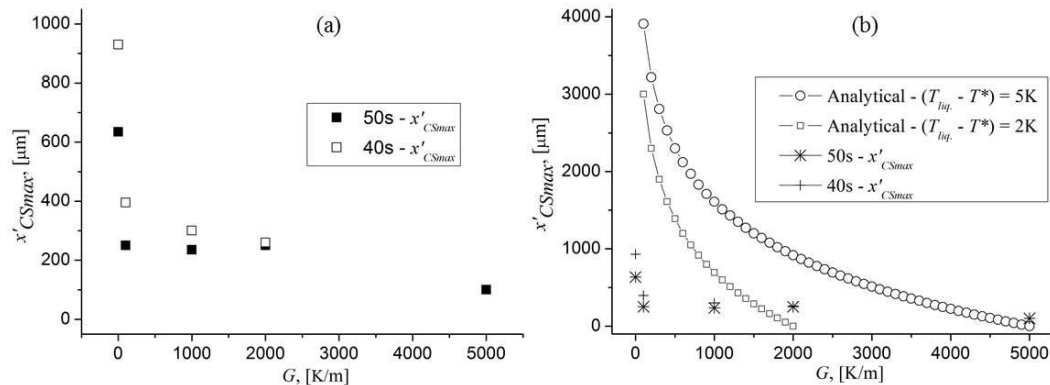


Figure 5. (a) x'_{CSmax} corresponding to ΔT_{CSmax} at $t = 40s$ and $50s$ from the numerical model, evaluated as $T_E - T_A$. (b) Comparison of analytical and numerical models. The general trend is similar although the analytical model shows much higher values of x'_{CSmax} .

The decrease in x'_{CSZ} and x'_{CSmax} represents a decrease in the size of the CSZ with increase in the thermal gradient. This is due to a greater increase in the temperature ahead of the growing interface. Moreover, a very steep gradient (see T_{A5} in figure 1) may result in no nucleation ahead of the interface. This is seen as $x'_{CSmax} \rightarrow 0$ in the analytical solution in figure 2b. On the other hand, the results from the numerical model in figure 4 show that the degree of supercooling, ΔT_{CS} , may also be a function of the time of solidification. Depending upon the amount of grain growth, x'_{CSmax} may not be fully developed (e.g. $G = 5000$ K/m, $t = 50s$) and, therefore, the supercooling achieved may be insufficient. Indeed, the analysis has shown that an increase in the amount of grain growth results in a proportional increase in x'_{CSmax} . The implication of this is that the potent particle distribution may assume a critical role in the subsequent nucleation events. From qualitative analysis, in general, a system with a steeper gradient with fully developed growing equiaxed grains may require a higher density of potent particles to trigger sufficient nucleation for a fine equiaxed grain structure.

Acknowledgements

DStJ and AP acknowledge the support of ARC Discovery Grant DP120101672 and the Centre for Advanced Materials Processing and Manufacturing (AMPAM) at UQ. PDL, LY acknowledge the Manchester X-ray Imaging Facility and the Research Complex at Harwell, funded in part by the EPSRC (EP/I02249X/1). Financial support from the ExoMet Project, which is co-funded by the European Commission in the 7th Framework Programme (contract FP7-NMP3-LA-2012-280421), by the European Space Agency and by the individual partner organisations is also acknowledged.

References

- [1] Easton M A and StJohn D H *Acta Materialia* 2001 **49** 1867
- [2] Easton M and StJohn D *Metallurgical and Materials Transactions A* 2005 **36A** 1911
- [3] Qian M, Cao P, Easton M A, McDonald S D and StJohn D H *Acta Materialia* 2010 **58** 3262
- [4] StJohn D H, Qian M, Easton M A and Cao P *Acta Materialia* 2011 **59** 4907
- [5] Wang W, Lee P D and McLean M *Acta Materialia* 2003 **51** 2971

- [6] Yuan L and Lee P D *Modelling and Simulation in Materials Science and Engineering* 2010 **18**
- [7] Dong H B and Lee P D *Acta Materialia* 2005 **53** 659
- [8] Badillo A and Beckermann C *Acta Materialia* 2006 **54** 2015
- [9] Prasad A, Yuan L, Lee P D and StJohn D H *Acta Materialia* 2013 **61** 5914
- [10] Atwood R C and Lee P D *Acta Materialia* 2003 **51** 5447
- [11] Atwood R C, Sridhar S and Lee P D *Scripta Materialia* 1999 **41** 1255